Dual-loop control strategy applied to the cluster of multiple nanogrids for rural electrification applications

Nasir, Mashood; Anees , Muhammad; Khan, Hassan Abbas; Guerrero, Josep M.

Published in:
IET Smart Grid

DOI (link to publication from Publisher):
10.1049/iet-stg.2019.0098

Publication date:
2019

Document Version
Accepted author manuscript, peer reviewed version

Dual–loop Control Strategy applied to the Cluster of Multiple Nanogrids for Rural Electrification Applications

Mashood Nasir [1*], Muhammad Anees [1], Hassan Abbas Khan [1], Josep M. Guerrero[2]

[1] Department of Electrical Engineering, Lahore University of Management Sciences, Lahore, Pakistan.
[2] Department of Energy Technology, Aalborg University, Aalborg, Denmark.
[*]mashood.nasir@lums.edu.pk

Abstract: In this paper, a dual-loop control strategy is applied to a highly distributed architecture of PV/battery based DC microgrid built through an interconnection of a cluster of multiple nanogrids. Typically, in these distributed architectures, resource sharing among the spatially distributed nanogrids is enabled via communication-based control methodologies, which adds cost and complexity to the overall system. Alternately, a communication-less and decentralized control methodology is proposed which utilizes inner loop current control and outer loop voltage droop (*V-I* droop) control for the coordinated resource sharing among the distributed resources. The proposed control scheme adapts various modes based upon the local measurements of bus voltage and battery state of charge, therefore, offers a distributed solution, omitting the need for centralized communication control. Various scenarios of power-sharing among the contributing nanogrids are evaluated through the proposed multi-mode adaptive control. The efficacy of the proposed control scheme is validated through simulations on MATLAB/Simulink and laboratory scale hardware prototype. Results show that the proposed decentralized control strategy is capable to ensure stable and coordinated operation without any dedicated layer of communication among the dispersed generation/storage resources.

1. Introduction

Access to electricity plays an important role in enhancing the socio-economic growth of a community [1]. Reliable access to electricity is extremely crucial for human well-being and can contribute to better health, employment, agriculture, and education opportunities. On the contrary, unavailability of electricity hampers the basic human rights including access to clean drinking water, proper lighting, and sustainable employment opportunities, therefore, declines the socio-economic status and tends to enhance the poverty [2]. According to the international energy agency (IEA), over 1 billion people i.e. 14 % of the global population do not have access to electricity [3]. The inhabitants of these regions rely on unhealthy resources such as kerosene oil for lighting and other applications causing many adverse effects on individuals as well as environment [4, 5]. Therefore, a higher focus on clean electrification is seen in recent years to help many developing regions attain access to electricity and subsequent sustainable development.

Solar photovoltaic (PV) and battery-based islanded DC microgrids are becoming very popular for the off-grid electrification due to decreasing PV costs as well as higher efficiency distributed generation [6-8]. Currently, commercial deployments either use a) centralized architecture with PV generation and battery storage at a centralized location) or b) distributed architecture with either generation or storage or both are spatially distributed) [9]. Centralized architectures have an advantage from installation, control, operation, and maintenance perspective. However, these have high distribution losses for higher power delivery [10, 11]. Moreover, these architectures need centralized planning at the very outset requiring large upfront system costs [12]. Prominent centralized installations include plants in Chhattisgarh, Sunderbans and Lakshadweep in India [13, 14]. Similarly, Mera Gao Power (MGP) in Utter Pradesh, India and the Jabula project in Cape Town, South Africa are other successful models of electrification via PV/battery-based islanded DC micro-grids [15].

Distributed architectures can have partially or highly distributed architectures where generation, as well as storage, can be distributed spatially. These systems have lower distribution losses and are generally scalable compared to rigidly centralized architectures [16-18]. Their modular nature imparts scalability to the overall microgrid structure, thereby; centralized planning and upfront installation of resources are not mandatory for these distributed architectures. Rather, in such topologies, multiple household-level energy systems are interconnected to formulate a microgrid, where each household may operate independently as well as in coordination. Further, these systems can have provisions of sharing power at the neighborhood level with the capability to extract the benefit of usage diversity at a village scale [19]. However, these systems typically require sophisticated control techniques involving communication among the distributed resources for their stable and coordinated operation. The involvement of dedicated communication resources will not only adds to the cost of the system but will also enhance the complexity of operation. From the perspective of rural electrification, such a complex and cost prohibitive solution is generally considered unviable for wide-scale adaption.

Various communication-less control schemes have been presented in the literature. For instance, Mashood *et. al* [17] presented a hysteresis based voltage droop algorithm that adjusts the duty cycle of interfacing converters for stable operation of the distributed microgrid. However, it does not consider the coordinated resource sharing and every contributing node supplies or receives a constant amount of power irrespective of its own resource availability.

A dual loop adaptive droop control scheme presented by Xiaonan *et al.* [20] considers the partial coordination of distributed resources proportional to the battery state of charge (*SOC*) index during power supply mode (battery discharge mode). However, it does not consider power-sharing in proportional to the *SOC* index during the charging mode of the battery. This results in suboptimal operation where all discharged batteries will get charged at the same rate irrespective of their resource deficiency. Also, the proposed scheme causes excessive distribution losses for unwanted SOC balancing and undesired charging / discharging of batteries in various households.

Subsequently, Mashood *et. al* [21] presented a fully coordinated adaptive droop scheme that considers resource sharing in proportional to SOC index for both charging and discharging modes. This scheme has an advantage as it employs an adaptive *I-V* droop method which has superior transient performance in comparison to the *V-I* droop method. However, the stability margins for *I-V* droop control are relatively smaller in comparison to *V-I* droop control, therefore, it may be subjected to instability due to the involvement of multiple constant power loads in the microgrid structure [22, 23].

In order to rectify these stability limitations, and enable communication-less resource sharing in a coordinated manner, an adaptive dual loop control strategy has been presented in [24]. This decentralized scheme employs *V-I* droop control for enhanced stability margins through configuring *V-I* droop, as a function of SOC index of the contributing battery. This results in each node contributing to power-sharing, in accordance with its resource availability. However, [24] discusses only the dual loop control of the bidirectional converter (responsible for power sharing among multiple nanogrids) without highlighting the control schematics for the solar converter (responsible for optimal power extraction from PV panel). Therefore, it does not consider the operation of the microgrid in extreme condition i.e. when excessive solar resources are available, while nanogrid load demand is minimal and microgrid voltage is at its saturation limit. If solar PV generation through solar converter is not controlled in such extreme conditions, it may result in the system overvoltages and may also instigate instability in the microgrid system. Moreover, [24] presents only simulation results, without their validation on a hardware platform. Alternatively, in this work, we have extended the control modes through the local coordination of solar converter (responsible for optimal power extraction from the solar panel) with the bidirectional converter (responsible for power sharing among neighboring nanogrids) to handle the extreme conditions of operation. This extended coordination among the nanogrid converters and controlled power generation from Solar PV results in enhanced stability of the system as demonstrated through simulation results. Moreover, a hardware prototype is developed and simulation results for the extended control are validated through laboratory scale hardware prototype.

The rest of the paper is organized as follows: Section II highlights the structure of the highly distributed PV/battery-based DC microgrid and its individual components. Section III presents the multimode algorithm along with decentralized control schematics for both of the converters in an individual nanogrid. Section IV presents the simulation and hardware results for various possible power-sharing scenarios. Based on the results, conclusions are drawn in section V.

2. Microgrid Architecture as an Interconnection of Nanogrids Cluster

Fig. 1 shows a highly distributed architecture of solar PV DC microgrid built through an interconnection of a cluster of *N* nanogrids [17]. An individual household in a village having its own PV generation, battery storage, solar converter and DC loads can be termed as a nanogrid. These nanogrids can be integrated through a bidirectional converter and DC bus to formulate a village scale microgrid where multiple nanogrids can exchange resources based upon their local requirements. Each household/nanogrid has two converters, where *Conv* a_i is the solar converter responsible for optimal power extraction from PV and *Conv* b_i is the interface converter, responsible for the bidirectional exchange of power between multiple households through DC bus. Each nanogrid can work independently as well as can share its resources with the neighboring nanogrids. The battery act as a buffer and provides a balance between PV power generation P^{PV}, local load consumption P^{L} and power transferred to or from the interconnecting DC bus P^{G}. The overall energy balance at i^{th} nanogrid can be represented in terms of battery state of charge SOC_i through energy balance equation.

$$SOC_i(t) = SOC_i^0 + \frac{1}{C_i}\int_0^T \left(P_i^{PV} - P_i^{L} - P_i^{G}\right) dt \qquad (1)$$

Where C_i is the energy capacity (Wh) of the battery installed in the i^{th} nanogrid and SOC_i^o is its initial state of charge. *SOC* act as a key indicator for energy resource availability in an individual nanogrid and multi-mode adaptive algorithm is therefore based upon this parameter. Another important parameter indicating the energy resource availability in overall microgrid network is DC bus voltage V^B and therefore, the multi-mode adaptive algorithm also takes into account while deciding the mode of operation and associated power sharing. Since both of these parameters are available locally at each nanogrid, therefore, a control algorithm based upon these two parameters will omit the need of centralized communication controller and the desired coordination will be achieved through decentralized control. The coordinated resource sharing feature is enabled via proposed adaptive dual loop control (inner current and outer voltage loop) of the bi-directional converter *Conv* b_i and is detailed in the next section. To tackle the excessive power generation conditions when PV generation is more than the battery capacity or local load requirements, the control of solar converter *Conv* a_i also adapts multiple modes based upon these two parameters. The extended control modes for *Conv* a_i is also discussed in the next section.

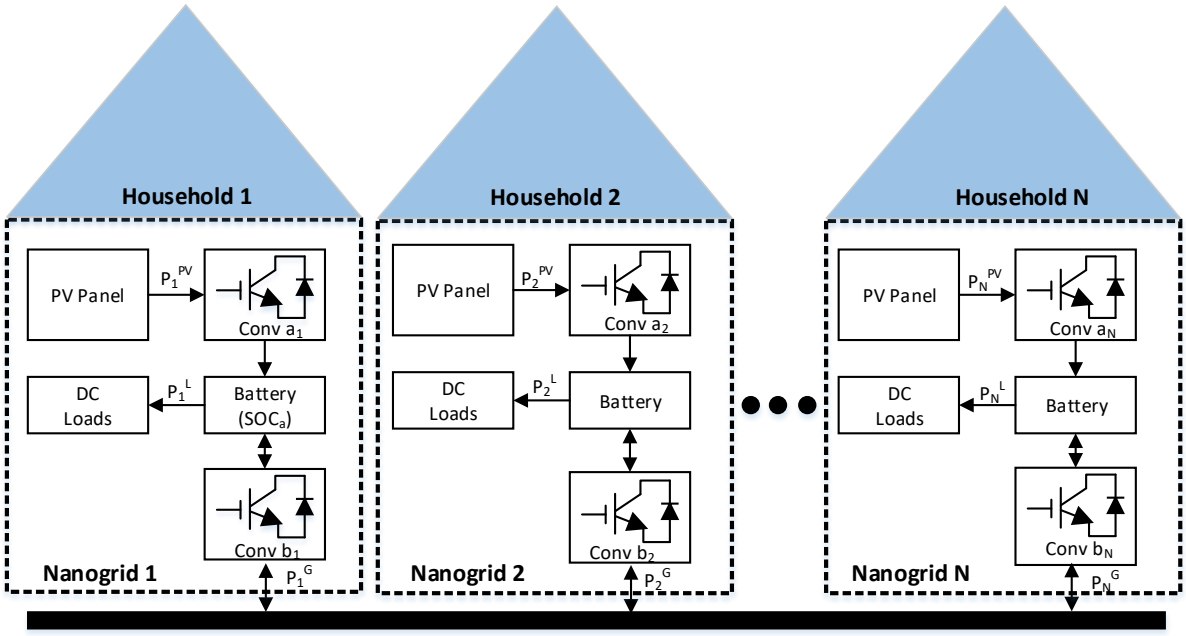

Fig. 1. *DC microgrid Architecture built through the interconnection of a cluster of multiple nanogrids*

3. Decentralized Control Algorithm

Based upon the local measurements of SOC_i and DC bus voltage V^B at i^{th} nanogrid, solar converter *Conv* a_i and the bidirectional interface converter *Conv* b_i can adapt the following modes.

3.1. Control Scheme for Solar Converter Conv ai

The power electronic circuit, control diagram and multiple modes adapted by solar converter *Conv* a_i during different modes of operation are shown in fig. 2. These modes are dictated by battery *SOC* and DC bus voltage V^B. Based upon the battery capacity, maximum and minimum thresholds on battery *SOC* i.e. SOC_{max} *and* SOC_{min} are defined. A value of *SOC* below SOC_{min} indicates that nanogrid energy availability is low and battery needs to be charged, while, a value of *SOC* above SOC_{max} indicates that excessive energy for neighborhood-level exchange is available.

The algorithm processes PV panel voltage V_i^{PV} and current I_i^{PV} for optimal power extraction from the PV panel at a given solar irradiance. During normal operating conditions when household requirements are higher than solar PV generation or battery is not fully charged, i.e. $SOC_i < SOC_{max}$ solar converter operates in maximum power point tracking (MPPT) mode. Various MPPT algorithms for optimal solar power extraction under uniform and non-uniform irradiance conditions are discussed in the literature [25, 26], however, in this work perturb and observe (P&O) is used due to its inherent simplicity and ease of applicability [25]. A value of $SOC_i > SOC_{max}$ indicates high resource availability in nanogrid, therefore, at this point another indication i.e. DC bus voltage V^B will determine the mode of operation. If DC bus voltage is below then the allowable saturation limit V^H, it indicates that other nanogrids are not saturated in terms of resource availability so the solar converter will continue its operation in MPPT mode. As soon as DC bus voltage will reach its maximum limit i.e. V^H, the solar converter will change its mode of operation from MPPT mode to current control mode (CCM) such that it will generate only the required amount of the current I_i^{load} and power P^L demanded by the local load. So, the solar converter will limit its generation according to the local requirements and avoid any overvoltage instability during excessive power generation condition.

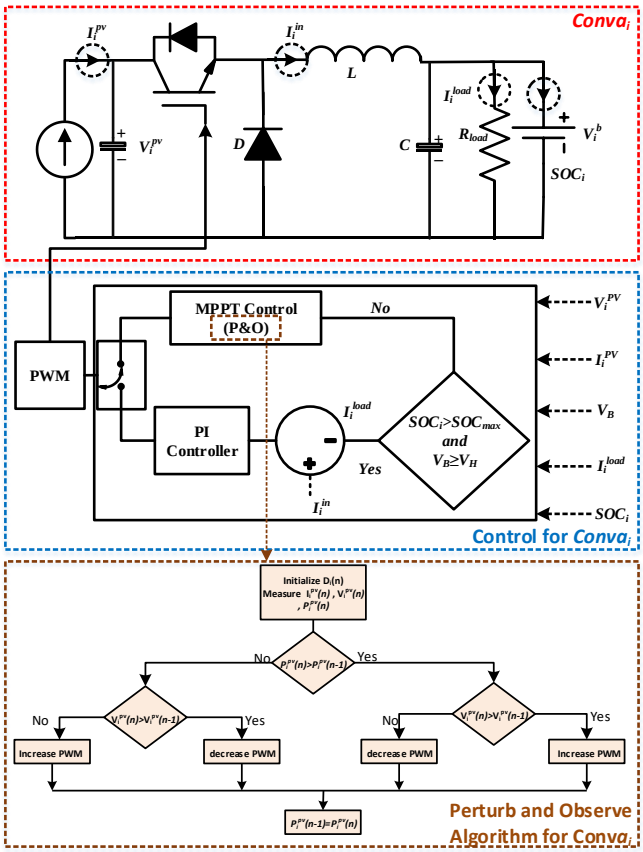

Fig. 2. *Power electronic circuit and multi-mode control scheme for Solar Converter*

3.2. *Control Scheme for bidirectional Interface Converter Conv bi*

The power electronic converter circuit, control diagram and multiple modes adapted by solar converter *Conv* a_i during different modes of operation are shown in fig. 3. In order to interconnect multiple households without any physical communication layer among the dispersed resources, an adaptive control scheme is used for each bidirectional converter *Conv* b_i. Based upon localized measurements of bus voltage V^B and battery *SOC* converter may shifts its mode of operation between a) Current Controlled Charging Mode, b) Current Controlled Discharging mode c) dual-loop adaptive *V-I* Droop mode, d) constant *I-V* droop mode. In each of these four modes, a current reference I_{ref} is generated as governed by (3)-(10). The inner loop PI current controller then generates the duty cycle *D* such that the desired current reference is achieved and the battery is charged or discharged at the desired value of current.

$$D = K_{p,i}\left(I_{ref} - I_{in}\right) + K_{i,i}\int_0^t \left(I_{ref} - I_{in}\right)dt \qquad (2)$$

Where, $K_{p,i}$ and $K_{i,i}$ are the proportional and integral constants for inner current loop PI controller and I_{in} is the inductor current of the bi-directional converter at which battery is charged or discharged. Thus, by controlling the current sharing of each individual household based upon the adaptive control strategy, a decentralized control ensuring stable and coordinated operation of the microgrid is achieved.

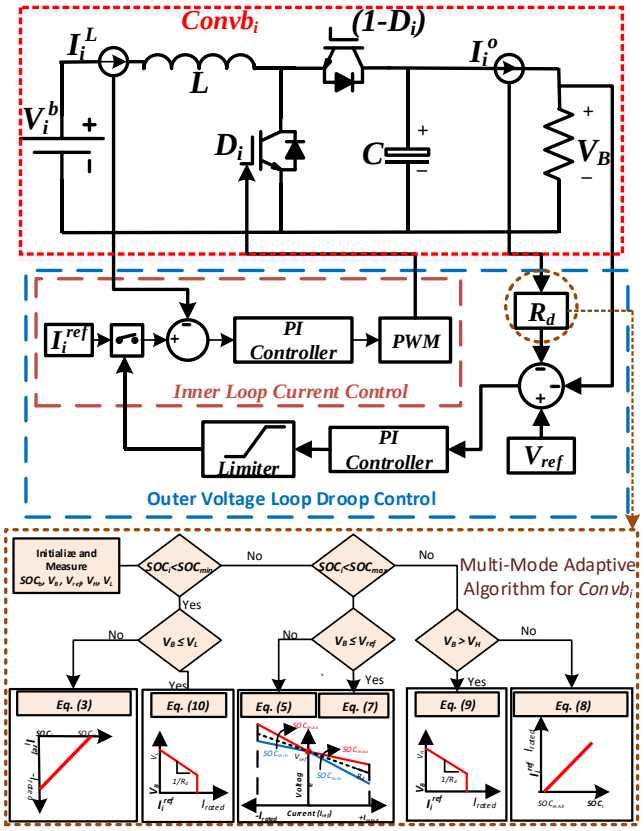

Fig. 3. *Power electronic circuit and multi-mode control scheme for bidirectional interface converter*

3.2.1 Current Controlled Charging Mode: *SOC* index of the battery serves as an indicator of the resource availability in an individual nanogrid. Similarly, DC bus voltage V^B serves as an indicator of the resource availability in the overall microgrid structure. When *SOC* falls below the minimum threshold, i.e. $SOC < SOC_{min}$, but $V^B > V^L$, i.e. DC bus voltage is higher than the minimum allowable V^L, bidirectional interface converter switches in current controlled charging mode (CCCM). The current reference is generated based upon the extent of resource deficiency such that it demands rated current I_{rated} when it is away from SOC_{min} and its current demand decreases as its SOC reaches to SOC_{min}. The PI controller then generates the duty cycle such that the desired current reference is achieved and the battery is charged at the desired value of current governed by (3).

$$I_{ref} = I_{rated}\left(\frac{SOC}{SOC_{\min}} - 1\right) \qquad (3)$$

3.2.2 Dual loop Adaptive Voltage Droop Control (V-I) Mode: In the intermediate range of *SOC*, i.e. $SOC_{min} \le SOC \le SOC_{max}$ each household has sufficient resource availability, therefore, it can either supply or demand power based upon the requirements of neighboring households. DC bus voltage V^B again serves as an indicator of the requirements of neighboring households. A value of V^B below the reference voltage V_{ref} indicates that one or more neighboring houses in the microgrid structure are deficient in resources and they need to be charged. At this point, the households having higher resource availability i.e. having higher *SOC* index should supply more power in comparison to those households which have relatively lower resource availability. This coordination is ensured through a modified discharging droop R_{dis} given by (4), whose visual depiction is also shown in Fig. 3.

$$R_{dis} = R_d\left[1 - 0.5\left(\frac{SOC - SOC_{\min}}{SOC_{\max} - SOC_{\min}}\right)\right] \qquad (4)$$

R_{dis} ensures that virtual droop impedance R_d which is generally considered constant in a conventional *V-I* droop is decreasing here in a linear fashion from R_d to $0.5R_d$ when *SOC* varies from SOC_{min} to SOC_{max}. Based upon this varying droop function R_{dis}, an outer voltage droop loop generates a reference for an inner loop current control as shown in Fig. 3 and given by (5).

$$I_{ref} = K_{p,v}\left(V_{ref} - V_o - I_o R_{dis}\right) + K_{i,v}\left(V_{ref} - V_o - I_o R_{dis}\right) \qquad (5)$$

Where, $K_{p,v}$ and $K_{i,v}$ are the proportional and integral constants for outer voltage loop PI controller and I_o is the output current of the bi-directional converter towards DC bus. Similarly, V^B above the reference voltage V_{ref} indicates that one or more neighboring houses are already saturated and they need to be discharged. Therefore, in this situation, the households having lower resource availability i.e. having lower SOC index should receive more power in comparison to those households which have relatively higher resource availability. This coordination is ensured through a modified

charging droop R_{ch} given by (6), whose visual depiction is also shown in Fig. 3.

$$R_{ch} = 0.5R_d\left[1+\left(\frac{SOC - SOC_{\min}}{SOC_{\max} - SOC_{\min}}\right)\right] \quad (6)$$

R_{dis} ensures that virtual droop impedance R_d which is generally considered constant in a conventional *V-I* droop is increasing here in a linear fashion from $0.5R_d$ to R_d when *SOC* varies from SOC_{min} to SOC_{max}. Based upon this varying droop function R_{ch}, an outer voltage droop loop generates a reference for an inner loop current control as shown in Fig. 2 and given by (6).

$$I_{ref} = K_{p,v}\left(V_{ref} - V_o - I_o R_{ch}\right) + K_{i,v}\left(V_{ref} - V_o - I_o R_{ch}\right) \quad (7)$$

Where, $K_{p,v}$ and $K_{i,v}$ are the proportional and integral constants for outer voltage loop PI controller and I_o is the input current of the bi-directional converter from DC bus.

Fig. 3 shows the variations of *V-I* droop as a function of *SOC*. It can be seen that for positive values of current I_{ref}, i.e. when an individual household is supplying power, moving from SOC_{min} to SOC_{max} decreases the slope of *V-I* curve and therefore, a household with a higher value of *SOC* supply more power in comparison to household having a lower value of *SOC*. Similarly, for negative values of current I_{ref}, i.e. when an individual household is receiving power, moving from SOC_{min} to SOC_{max} increases the slope of *V-I* curve and therefore, a household with a lower value of *SOC* receives more power in comparison to household having a higher value of SOC and vice versa.

3.2.3 Current Controlled Discharging Mode: When, *SOC* of the battery in an individual household increases above maximum threshold due to higher incident solar irradiance and associated PV power generation, i.e. $SOC > SOC_{max}$, and the neighboring nanogrids have the capacity to absorb the excessive power, i.e. $V^B < V^H$, its bidirectional converter switches in current controlled discharging mode (CCDM). The current reference is generated based upon the extent of resource saturation such that it supplies rated current I_{rated} when it is away from SOC_{max} and its current supply decreases as its *SOC* reaches to SOC_{max}. The PI controller then generates the duty cycle such that the desired current reference is achieved and the battery is discharged at the desired value of current governed by (8).

$$I_{ref} = I_{rated}\left(\frac{SOC_i - SOC_{\max}}{100 - SOC_{\max}}\right) \quad (8).$$

3.2.3 Constant I-V Droop Mode: Extreme operation conditions occur when solar PV generation is much higher than local as well as global load requirements i.e. when $SOC > SOC_{max}$ and $V^B > V^H$ or when PV generation and battery storage energy is lower than load requirements, i.e. when $SOC < SOC_{max}$ and $V^B < V^L$. In these extreme conditions bidirectional interface converter switches in constant I-V droop mode, thereby fixing the DC bus voltage at allowable limits i.e. V^H or V^L. The current reference in these extreme conditions is given by (9) and (10) respectively. It is important to reiterate that in excessive generation condition solar converter changes its mode of operation from MPPT to current control mode, while in case of low generation extreme condition, a relay is used to disconnect the load and enforce load shedding.

$$I^{ref} = \frac{1}{R_d}\left(V_H - V_B\right) \;;\; \text{if } V_B \geq V_H \quad (9)$$

$$I^{ref} = \frac{1}{R_d}\left(V_L - V_B\right) \;;\; \text{if } V_B \leq V_L \quad (10)$$

4. Results and Discussions

For the validation of the proposed control scheme and associated power coordination, various test cases are analyzed via simulations and laboratory scale hardware prototype.

4.1. Simulation Results

For the validation of the proposed control scheme, simulations are carried out in MATLAB/ Simulink using physical models of the converters and control schematic shown in Figs. 2 and 3. Various parameters for simulation are also shown in Table 1. The droop value R_d is selected according to the converter ratings and adjusted such that voltage of the microgrid is stable for its full range of operation. Similarly, integral and proportional parameters for current loop and voltage loop controllers are chosen based upon the closed-loop stability of the proposed scheme.

4.1.1 One House is in CCCM and Remaining Houses are in V-I Droop Mode: In this scenario, battery of house 1 is assumed below minimum threshold of *SOC i.e.* SOC_1=10%, while the batteries of the other three households are assumed within the specified maximum and minimum thresholds, i.e. SOC_2=35%, SOC_3=55%, SOC_4=75%. The results of current sharing through the proposed decentralized control scheme are shown in Fig. 4. From Fig. 4, it can be seen that house 1 is demanding power in proportion to its resource deficiency as governed by (3), while house 2, 3 and 4 are supplying power in proportion to their resource availability such that house 4 having highest resource availability (*SOC* index) is supplying highest amount of current and house 2 is supplying lowest value of current for charging the battery of house 1.

Table 1 Parameters of simulated case study

Description of the Parameter	Value
No. of Nanogrids/ households	4
The input capacitance of each *Conv* b_i	220µF
Inductance of each *Conv* b_i	2.1mH
The inductance of each *Conv* a_i	500µH
DC Bus capacitance	10mF
Switching frequency for *Conv* a_i and *Conv* b_i	10kHz
Battery capacity for each household	2400Wh
Rated Charging current for the battery	10A
Rated voltage of each battery	24V
Maximum threshold of battery SOC	80%
Minimum threshold of battery SOC	30%
The reference voltage for DC bus	48V
Initial Voltage of DC bus	24V
Droop Coefficient for each *Conv* a_i	0.21Ω
Droop Coefficient for each *Conv* b_i	0.23Ω
Parameters of Current loop Controller	0.33, 15
Parameters of Voltage loop Controller	1.75, 10

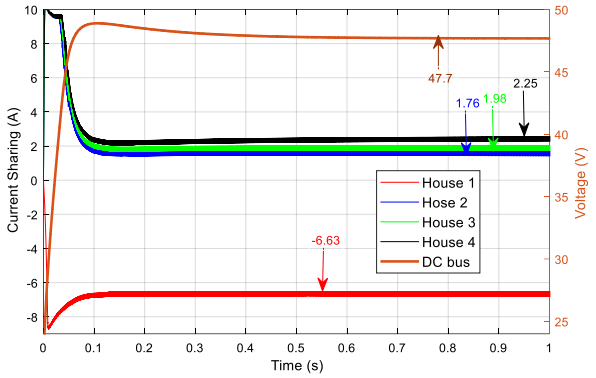

Fig. 4. *Simulation Results for Current Sharing and DC bus Voltage in case 1.*

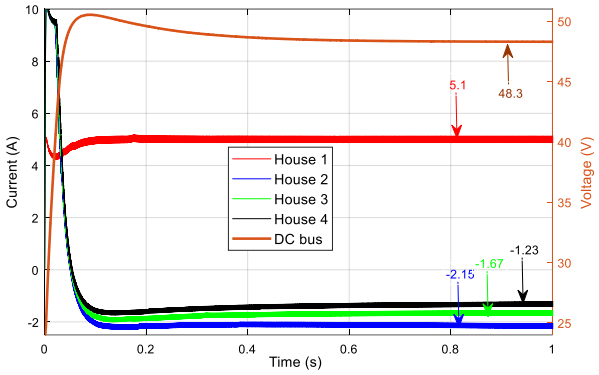

Fig. 5. *Simulation Results for Current Sharing and DC bus Voltage in case 2.*

4.1.2 One House is in CCDM and Remaining Houses are in V-I Droop Mode: In this scenario, battery of house 1 is assumed above maximum threshold of *SOC i.e.* SOC_1=90%, while the batteries of the other three households are assumed within the specified maximum and minimum thresholds of *SOC* i.e. SOC_2=35%, SOC_3=55%, SOC_4=75%. The results of current sharing through the proposed decentralized control scheme are shown in Fig. 5. From Fig. 5, it can be seen that house 1 is supplying power in proportion to its resource saturation as governed by (8), while house 2, 3 and 4 are absorbing power in proportion to their resource deficiency such that house 2 having lowest resource availability (*SOC* index) is receiving highest amount of current and house 4 is receiving lowest value of current for charging their batteries from house 1.

4.1.3 One House is in CCCM, One House in CCDM and Remaining Houses are in V-I Droop mode: In this scenario, battery of house 1 is assumed below minimum threshold of *SOC i.e.* SOC_1=15%, battery of house 2 is assumed above minimum threshold of *SOC i.e.* SOC_1=95%, while the batteries of the other two households are assumed within the specified maximum and minimum thresholds of *SOC* i.e. SOC_3=55%, SOC_4=75%. The results of current sharing through the proposed decentralized control scheme are shown in Fig. 6. From Fig. 6, it can be seen that house 1 is demanding power in proportion to its resource deficiency as governed by (3), house 2 is supplying power in proportion to its resource saturation as governed by (8).

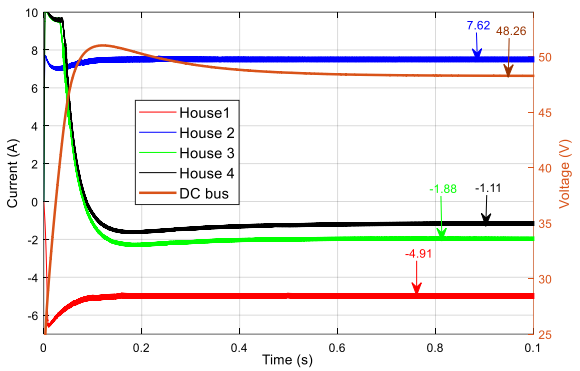

Fig. 6. *Simulation Results for Current Sharing and DC bus Voltage in case 3.*

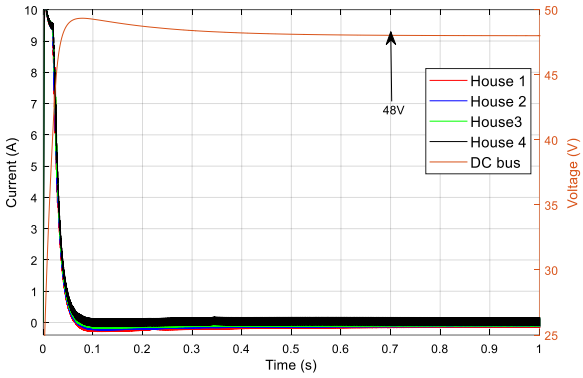

Fig. 7. *Simulation Results for Current Sharing and DC bus Voltage in case 4.*

In this scenario, houses 3 and 4 will supply/demand power in accordance with the net current supplied at DC bus and its resulting voltage. Since in this scenario net current supplied by house 2 is higher than the current absorbed by house 1, therefore, net voltage of DC bus is higher than V_{ref}, as a result of which house 3 and 4 are absorbing power in accordance with their resource deficiency such that household 2 being at lower state of charge is being charged at relatively higher current in comparison to household 3 as shown by Fig. 6.

4.1.4 All Four Houses are in V-I Droop Mode: In this scenario, all four houses are assumed within the maximum and minimum threshold range of *SOC*. Results of current sharing and dc bus voltage are shown in Fig. 7. Since all the houses are self-sufficient and are operating in *V-I* droop mode; therefore voltage is stable at V_{ref} and there is no net power flow from one household to other via DC bus. In an optimally sized DC microgrid [27], households will be operating in this mode for most of the times, therefore, distribution losses will be minimum from generation end to utilization end. This reduction in losses is otherwise not possible with the SOC balancing- based methodology presented in [20].

4.1.5 All Four Houses are in Constant I-V Droop Mode and Excessive Generation is Available: In this scenario, all four houses are assumed at the maximum *SOC* i.e. SOC_1=SOC_2=SOC_3=SOC_4=85%. As a result of which all households will try to supply power to the neighboring houses in accordance with (8). Consequently, grid voltage V^B will start increasing.

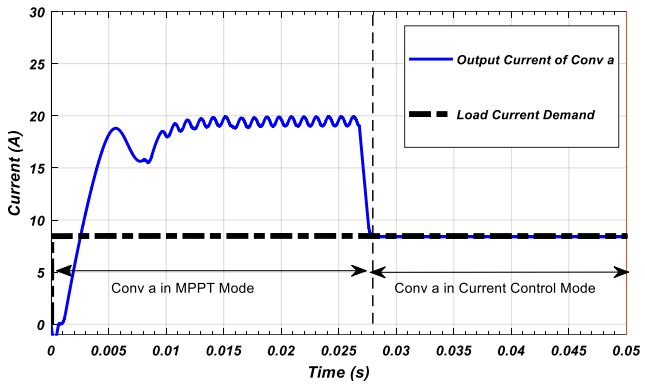

Fig. 8. *Simulation Results for the transition between MPPT and CCM in excessive generation condition.*

When V^B will attain its maximum allowable voltage i.e. V^H, *Conv* a_i will shift its mode of operation from MPPT mode to current controlled mode (CCM), while *Conv* b_i for each house will shift its mode to constant *I-V* droop mode given by (9). In this mode of operation, *Conv* a_i will curtail the PV power generation and associated current output from the converter in accordance with household load current demand. This transition between MPPT and CCM is shown in Fig. 8. For instance, in Fig. 8, a constant load current demand 0f 9A is considered. In the start of the simulation, when the converter is operating in MPPT mode, the current generated by PV is at MPP i.e. 20 A. At $t = 0.028$ *s* converter shifts its mode of operation and curtails current demand equal to household current demand i.e. 9 A. Therefore, this extended control allows the transition from MPPT mode to CCM and avoids overvoltage instability in excessive generation conditions.

4.2. *Hardware Results*

For the validation of the proposed control scheme, a laboratory scale hardware prototype is developed as shown in Fig. 9. The converters for two nanogrids are designed and the integration of two nanogrids is achieved through DC bus interconnection emulated via a large capacitor and battery as shown in Fig. 9. Various other hardware parameters are detailed in table 2. Various scenarios of power-sharing are evaluated using the proposed control algorithm and are discussed below.

Table 2 Parameters of hardware implementation

Description of the Parameter	**Value**
No. of Nanogrids/ households	2
Input capacitance of each *Conv* b_i	1000μF
The inductance of each *Conv* b_i	700μ H
The inductance of each *Conv* a_i	650μH
DC Bus capacitance	6.6mF
Switching frequency for converters	20kHz
Battery capacity for each household	1440Wh
Rated battery charging current	15A
Rated voltage of each battery	12V
Maximum threshold of battery SOC	80%
Minimum threshold of battery SOC	30%
The reference voltage for DC bus	48V
Converters droop coefficient	0.1 Ω
Micro-controller Specifications	DSPIC 30F4011
Grid Battery Specification	500 Wh

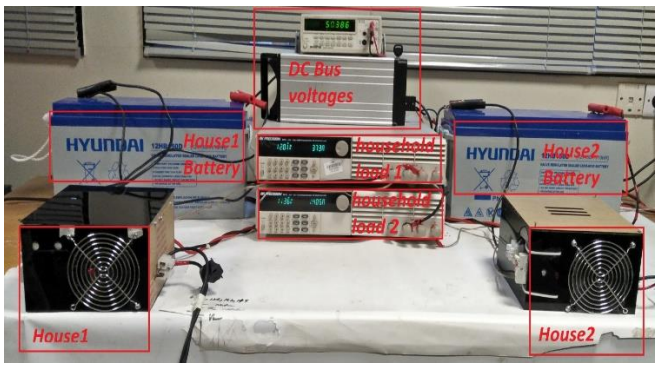

Fig. 9. *Laboratory scale hardware implementation setup.*

4.2.1 Both Houses are in V-I Droop mode and Grid is demanding Power: In this scenario, batteries of house 1 and house 2 are between the maximum and minimum thresholds of *SOC*, and the grid is demanding power i.e. $V^B < V_{ref}$. Two sub-cases are considered for the evaluation of coordinated power-sharing such that in case (a) SOC_2 =70 % > SOC_1 = 60 % and in case (b) $SOC_2 = SOC_1$ = 60%. In this scenario, both houses will contribute current for the grid battery charging based upon their resource availability. The resultant current sharing characteristics along with grid voltage profile for both cases is shown in Fig. 10 and 11 respectively.

From Figs. 10 and 11 it can be seen that in case (a), house 2 has relatively higher *SOC*, therefore, it is contributing a relatively higher amount of current in comparison to house 1, while in case (b), both houses are contributing almost equal current for grid battery charging.

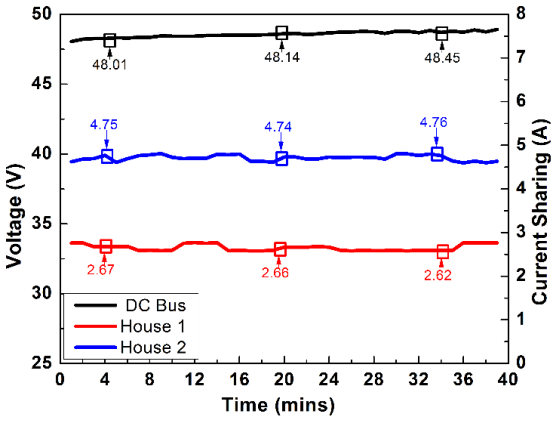

Fig. 10. *Hardware Results for Current Sharing and DC bus Voltage in Scenario 1, case (a).*

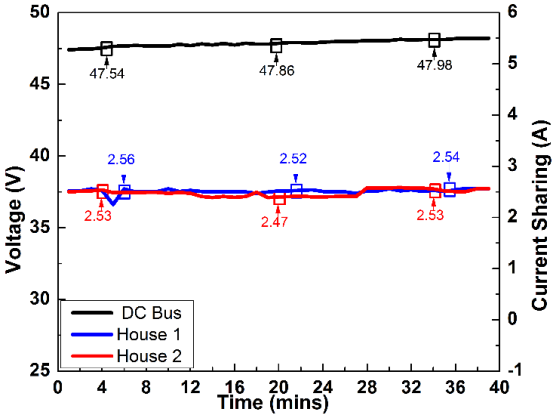

Fig. 11. *Hardware Results for Current Sharing and DC bus Voltage in Scenario 1, case (b).*

4.2.2 Both Houses are in V-I Droop mode and Grid is Supplying Power: In this scenario, batteries of house 1 and house 2 are assumed between the maximum and minimum thresholds of *SOC*, and the grid is supplying power i.e. $V^B > V_{ref}$. Two sub-cases are considered for the evaluation of coordinated power-sharing such that in case (a) SOC_2 =70 % > SOC_1 = 60 % and in case (b) $SOC_2 = SOC_1$ = 60%. In this scenario, both houses will absorb current from the grid battery charging based upon their resource availability. The resultant current sharing characteristics along with grid voltage profile for both cases is shown in Fig. 12 and 13 respectively.

From Figs. 12 and 13, it can be seen that in case (a), house 2 has relatively higher *SOC*, therefore, it is absorbing the relatively lower amount of current in comparison to house 1, while in case (b), both houses are absorbing almost equal current from the grid.

4.2.3 Both Houses are in I-V Droop mode and Excessive Generation is Available: In this scenario, batteries of both houses are above maximum threshold i.e. $SOC_1 = SOC_2$ = 90% and excessive PV generation is available. In this scenario, both houses will start supplying power to the grid until the grid voltage attains its maximum value. The current supplied by *Conv* a_1 is shown in Fig. 14. From Fig. 14, it can be seen that at *t = 23 minutes*, the solar converter changes its mode of operation from MPPT mode to current control mode and it curtails PV generation according to household current requirements i.e. around 5. 5 A.

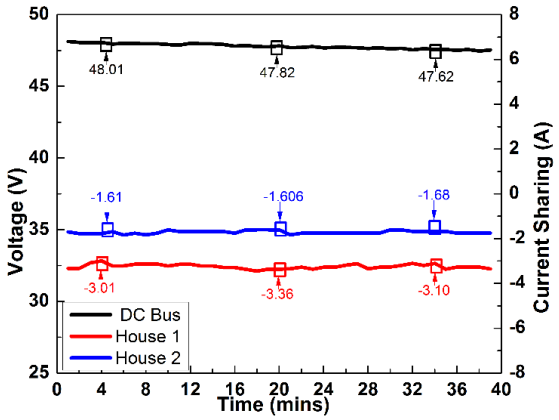

Fig. 12. *Hardware Results for Current Sharing and DC bus Voltage in Scenario 2, case (a).*

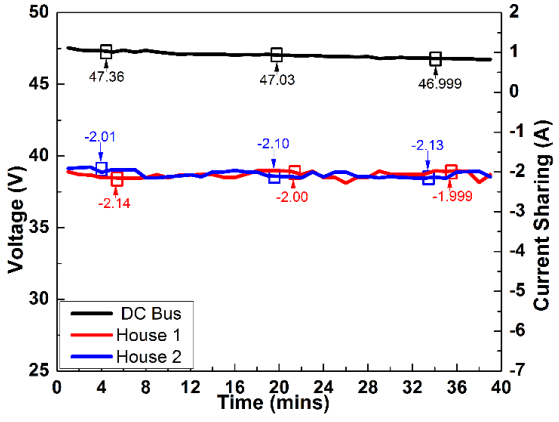

Fig. 13. *Hardware Results for Current Sharing and DC bus Voltage in Scenario 2, case (b).*

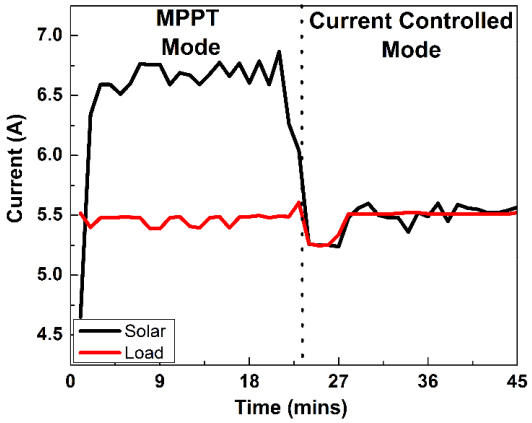

Fig. 14. *Hardware Results for the transition between MPPT and CCM in excessive generation condition.*

5. Conclusion

Distributed architectures of PV and battery based islanded DC microgrids are generally more suitable for rural electrification provided they have a decentralized control strategy. In this work, such an adaptive control scheme using dual loop *V-I* droop is presented and extended control modes for dealing with excessive PV generation conditions are also discussed. The validity of the proposed decentralized control scheme is demonstrated through simulated and measured results. V-I droop ensures higher stability margins, while *SOC* based variations in droop enable coordinated resource sharing without dedication communication resources. Therefore, distributed architecture with the proposed adaptive control scheme combines the advantage of both of the existing architectures i.e. a) lower distribution losses, b) scalability and modularity, c) communication-less coordinated control and d) stability over a wide range of operation and is deemed highly suitable for future rural electrification deployments.

6. References

[1] E. Bergasse, W. Paczynski, M. Dabrowski, and L. De Wulf, "The relationship between energy and socio-economic development in the Southern and Eastern Mediterranean," 2013.

[2] J. Peters and M. Sievert, "Impacts of rural electrification revisited–the African context," *Journal of Development Effectiveness*, vol. 8, pp. 327-345, 2016.

[3] World Energy Outlook (WEO, 2017), Electricity Access Database [Online]. Available: https://www.iea.org/publications/freepublications/publication/WEO2017SpecialReport_EnergyAccessOutlook.pdf

[4] M. González-Eguino, "Energy poverty: An overview," *Renewable and Sustainable Energy Reviews*, vol. 47, pp. 377-385, 2015.

[5] N. L. Lam, K. R. Smith, A. Gauthier, and M. N. Bates, "Kerosene: a review of household uses and their hazards in low-and middle-income countries," *Journal of Toxicology and Environmental Health, Part B*, vol. 15, pp. 396-432, 2012.

[6] D. Schnitzer, D. S. Lounsbury, J. P. Carvallo, R. Deshmukh, J. Apt, and D. M. Kammen, "Microgrids for Rural Electrification: A critical review of best practices based on seven case studies," *United Nations Foundation*, 2014.

[7] J. J. Justo, F. Mwasilu, J. Lee, and J.-W. Jung, "AC-microgrids versus DC-microgrids with distributed energy resources: A review," *Renewable and Sustainable Energy Reviews*, vol. 24, pp. 387-405, 2013.

[8] G. He and D. G. Victor, "Experiences and lessons from China's success in providing electricity for all," *Resources, Conservation and Recycling*, vol. 122, pp. 335-338, 2017.

[9] M. Nasir, H. A. Khan, N. A. Zaffar, J. C. Vasquez, and J. M. Guerrero, "Scalable Solar dc Micrigrids: On the Path to Revolutionizing the Electrification Architecture of Developing Communities," *IEEE Electrification Magazine*, vol. 6, pp. 63-72, 2018.

[10] M. Nasir, N. A. Zaffar, and H. A. Khan, "Analysis on central and distributed architectures of solar powered DC microgrids," in *Power Systems Conference (PSC), 2016 Clemson University*, 2016, pp. 1-6.

[11] M. Hamza, M. Shehroz, S. Fazal, M. Nasir, and H. A. Khan, "Design and analysis of solar PV based low-power low-voltage DC microgrid architectures for rural electrification," in *Power & Energy Society General Meeting, 2017 IEEE*, 2017, pp. 1-5.

[12] H. A. Khan, H. F. Ahmad, M. Nasir, M. F. Nadeem, and N. A. Zaffar, "Decentralised electric power delivery for rural electrification in Pakistan," *Energy policy*, vol. 120, pp. 312-323, 2018.

[13] S. Mishra and O. Ray, "Advances in nanogrid technology and its integration into rural electrification in India," in *Power Electronics Conference (IPEC-Hiroshima 2014-ECCE-ASIA), 2014 International*, 2014, pp. 2707-2713.

[14] D. Palit, G. K. Sarangi, and P. Krithika, "Energising Rural India Using Distributed Generation: The Case of Solar Mini-Grids in Chhattisgarh State, India," in *Mini-Grids for Rural Electrification of Developing Countries*, ed: Springer, 2014, pp. 313-342.

[15] J. Urpelainen, "Energy poverty and perceptions of solar power in marginalized communities: Survey evidence from Uttar Pradesh, India," *Renewable Energy*, vol. 85, pp. 534-539, 2016.

[16] W. Inam, D. Strawser, K. K. Afridi, R. J. Ram, and D. J. Perreault, "Architecture and system analysis of microgrids with peer-to-peer electricity sharing to create a marketplace which enables energy access," in *Power Electronics and ECCE Asia (ICPE-ECCE Asia), 2015 9th International Conference on*, 2015, pp. 464-469.

[17] M. Nasir, H. A. Khan, A. Hussain, L. Mateen, and N. A. Zaffar, "Solar PV-based scalable DC microgrid for rural electrification in developing regions," *IEEE Transactions on Sustainable Energy*, vol. 9, pp. 390-399, 2018.

[18] P. A. Madduri, J. Poon, J. Rosa, M. Podolsky, E. A. Brewer, and S. R. Sanders, "Scalable DC Microgrids for Rural Electrification in Emerging Regions," *IEEE Journal of Emerging and Selected Topics in Power Electronics*, vol. 4, pp. 1195-1205, 2016.

[19] S. Groh, D. Philipp, B. E. Lasch, and H. Kirchhoff, "Swarm electrification-Suggesting a paradigm change through building microgrids bottom-up," in *Developments in Renewable Energy Technology (ICDRET), 2014 3rd International Conference on the*, 2014, pp. 1-2.

[20] X. Lu, K. Sun, J. M. Guerrero, J. C. Vasquez, and L. Huang, "State-of-charge balance using adaptive droop control for distributed energy storage systems in DC microgrid applications," *IEEE Transactions on Industrial Electronics*, vol. 61, pp. 2804-2815, 2014.

[21] M. Nasir, Z. Jin, H. A. Khan, N. A. Zaffar, J. C. Vasquez, and J. M. Guerrero, "A decentralized control architecture applied to dc nanogrid clusters for rural electrification in developing regions," *IEEE Transactions on Power Electronics*, vol. 34, pp. 1773-1785, 2019.

[22] F. Gao, S. Bozhko, A. Costabeber, C. Patel, P. Wheeler, C. I. Hill, *et al.*, "Comparative stability analysis of droop control approaches in voltage-source-converter-based DC microgrids," *IEEE Transactions on Power Electronics*, vol. 32, pp. 2395-2415, 2017.

[23] Z. Jin, L. Meng, and J. M. Guerrero, "Comparative admittance-based analysis for different droop control approaches in DC microgrids," in *DC Microgrids (ICDCM), 2017 IEEE Second International Conference on*, 2017, pp. 515-522.

[24] M. Nasir, H. A. Khan, K. A. K. Niazi, Z. Jin, and J. M. Guerrero, "Dual–loop Control Strategy applied to PV/battery based Islanded DC microgrids for Swarm Electrification of Developing Regions," *Journal of Engineering*, 2018.

[25] B. Subudhi and R. Pradhan, "A comparative study on maximum power point tracking techniques for photovoltaic power systems," *Sustainable Energy, IEEE transactions on*, vol. 4, pp. 89-98, 2013.

[26] M. Nasir and M. F. Zia, "Global maximum power point tracking algorithm for photovoltaic systems under partial shading conditions," in *Power Electronics and Motion Control Conference and Exposition (PEMC), 2014 16th International*, 2014, pp. 667-672.

[27] M. Nasir, S. Iqbal, and H. A. Khan, "Optimal Planning and Design of Low-Voltage Low-Power Solar DC Microgrids," *IEEE Transactions on Power Systems*, vol. 33, pp. 2919-2928, 2018.